The magnetic properties of a $Gd_{72}Sc_{28}$ single crystal

1995 J. Phys.: Condens. Matter 7 9853

(http://iopscience.iop.org/0953-8984/7/50/019)

J. Phys.: Condens. Matter 7 (1995) 9853–9861. Printed in the UK

The magnetic properties of a $Gd_{72}Sc_{28}$ single crystal

M A Salgueiro da Silva†, J M Moreira†, J A Mendes†, V S Amaral†, J B Sousa† and S B Palmer‡

† Instituto de Física dos Materiais da Universidade Porto (IFIMUP-IMAT) and Centro de Física Universidade Porto (CFUP), Praça Gomes Teixeira, 4050 Porto, Portugal

‡ Physics Department, University of Warwick, Coventry CV4 7AL, UK

Received 1 June 1995

Abstract. We present a discussion of the magnetic properties and magnetic phase transitions of $Gd_{72}Sc_{28}$ monocrystalline alloys based on experimental results of the magnetization (M) and transport properties (ρ, $d\rho/dT$, $\Delta\rho/\rho$). In particular, a spin reorientation transition is observed in the canted ferromagnetic phase. Using dM/dH and $d(\Delta\rho/\rho)/dH$ data we have obtained the H–T magnetic phase diagram of this particular alloy composition as a function of basal plane applied magnetic field, H.

1. Introduction

The magnetic properties of the $Gd_{1-x}Sc_x$ alloys have been studied in some detail using measurements of single-crystal elastic constants to support neutron diffraction experiments [1–3]. The alloys are of interest due to the competition between the ferromagnetic order (F) developed in the Gd rich alloys and the helical antiferromagnetic order (HAF) developed in Sc rich alloys. This competition, when coupled with the low basal plane anisotropy, leads to a complex magnetic phase diagram, in particular in the vicinity of the critical composition $Gd_{74}Sc_{26}$.

A partial *zero-magnetic-field* phase diagram is shown in figure 1 where the points on the phase boundaries have been obtained by elastic constant measurements and the magnetic structure in the different phases determined by neutron diffraction measurements [3]. It can be seen that in the Sc rich alloys with $x > 35$ at.% the only magnetic phase in zero field is a basal plane helix and we have shown that for $x = 34$ at.% the turn angle of the helix (ω) locks on to a turn angle of 26° below 30 K.

As the Gd concentration is increased the basal plane helix transforms into a conical helix (or ferromagnetic spiral) at low temperatures. The addition of more Gd triggers a transition from the conical helix to a canted ferromagnetic phase, again at low temperatures, and transitions observed within this canted region can be attributed to spin reorientation effects. Above 78 at.% Gd the material displays only ferromagnetic behaviour.

The present paper describes a study of the magnetic properties of a- and c-axis monocrystals of the $Gd_{72}Sc_{28}$ alloys which display the three ordered magnetic phases *viz* a basal plane helix, a conical helix and a canted ferromagnet plus a spin reorientation transition within the canted ferromagnetic phase. Figure 2, based on neutron diffraction results, shows the angle (θ) that the spontaneous magnetization makes with the hexagonal c-axis in the various magnetic phases. The rapid change of θ with temperature in the conical helix phase is most unusual. In pure Gd one also observes a rapid change of this angle

0953-8984/95/509853+09$19.50

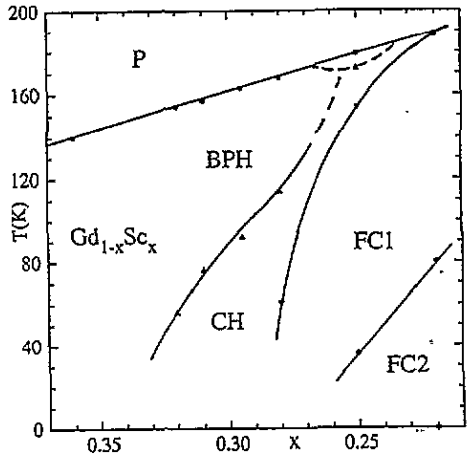

Figure 1. The zero-field partial magnetic phase diagram for Gd–Sc random monocrystalline alloys, P—paramagnetic; BPH—basal plane helix; CH—conical helix; FC—ferro canted phase.

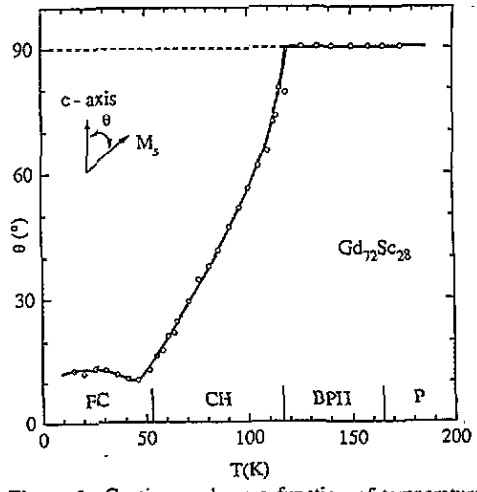

Figure 2. Canting angle as a function of temperature for $Gd_{72}Sc_{28}$.

with temperature but in the opposite direction, with $\theta = 0$ at high temperatures and rapidly rising below about 240 K, reaching $\theta \sim 70°$ for T around 200 K [4].

In addition to studying the behaviour of the zero-field magnetic properties in detail, we will also describe the phase diagram of this particular alloy composition *as a function of an applied basal plane field.* This diagram was obtained from complementary information provided by the following properties: magnetization $M(T, H)$, electrical resistivity (ρ, $d\rho/dT$) and magnetoresistance $\Delta\rho(T, H)/\rho(T, 0)$.

2. Experimental details

The $Gd_{72}Sc_{28}$ single crystal has been reported on in an earlier publication [5]. Samples were prepared in the form of cubes for ultrasonic measurements, and needles with the long axes parallel to either the c-axis or the basal plane, a-axis, for magnetization and transport property determinations. The ultrasonic measurements of the elastic constants were carried out by standard techniques [6] with a fully automated system [7], as were the transport properties [8, 9]. The magnetization was measured with a SQUID magnetometer with a sensitivity of 10^{-7} emu.

3. Results and discussion

3.1. Magnetization

The temperature dependence of the magnetic moment taken in an a-axis magnetic field of 50 Oe is shown in figure 3. The measurements were always taken on warming from low temperature and they delineate the various magnetic phases very clearly. One of the curves (ZFC) was obtained *after cooling* the sample in zero field from above T_N, whereas the other curve (FC) was obtained after cooling the sample in an applied field of 50 Oe. Qualitatively

both curves are similar, except for a small hysteresis developing at temperatures below $T^* \cong 110$ K.

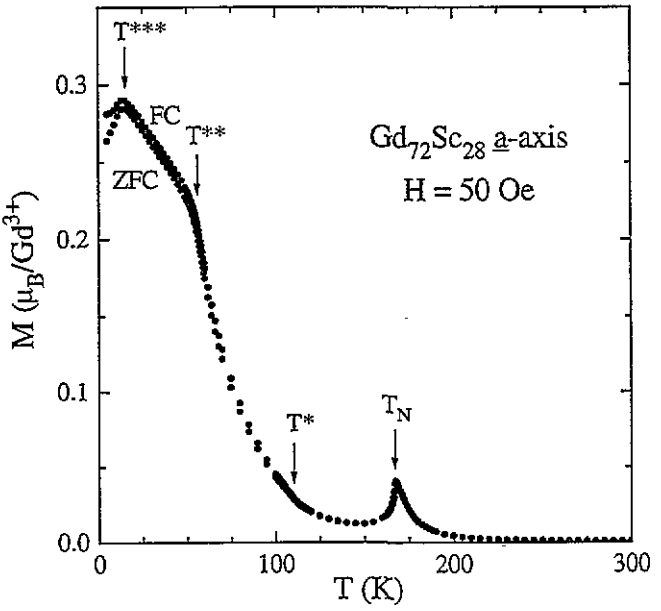

Figure 3. Isofield magnetization as a function of temperature for the a-axis $Gd_{72}Sc_{28}$ sample ($H_{//} = 50$ Oe).

The cusp at $T_N \cong 168$ K marks the onset of the basal plane helimagnetic phase, although there is already a hint of asymmetry in the cusp due to a precursor ordered phase stabilized by the applied field. The conical helix which occurs below T^* produces a pronounced increase in the magnetic moment, followed by a rapid decrease in slope at lower temperature as the canted ferromagnet becomes stabilized at $T^{**} \cong 55$ K. The final decrease in moment below $\cong$15 K may be indicative of the moment turning further towards the c-axis.

The isothermal magnetization curves for a-axis fields are shown in figure 4. Saturation is readily achieved at low temperatures with the moments easily rotating from the c-axis in the ferromagnetic canted phase. A magnetic moment of 7.16 μ_B per Gd formula unit is obtained, which is consistent with other Gd alloys [10] where the atomic moment of 7 μ_B is augmented by polarization effects of the conduction electrons.

The $M(H)$ curves obtained at higher temperatures, where helimagnetism occurs, show little difference in magnetization behaviour between the basal plane and the conical helices. The onset of the rapid increase in magnetization at the critical field $H = H_{c1}$ represents the destruction of the helix phase, with the transition to the fan magnetic structure. From these curves we have obtained accurate H_{c1} values to draw the corresponding $H_{c1}(T)$ curve shown in figure 8. It is more difficult to identify in $M(H)$ the second critical field (H_{c2}) where the fan phase collapses into ferromagnetism, so complementary magnetoresistance data ($\Delta\rho/\rho$) were also obtained (see below).

3.2. Electrical resistivity (ρ, $d\rho/dT$)

The temperature dependence of the resistivity ρ and its temperature derivative $d\rho/dT$ are shown in figure 5 for both the c- and a-axes. The effects of the electron interaction with the

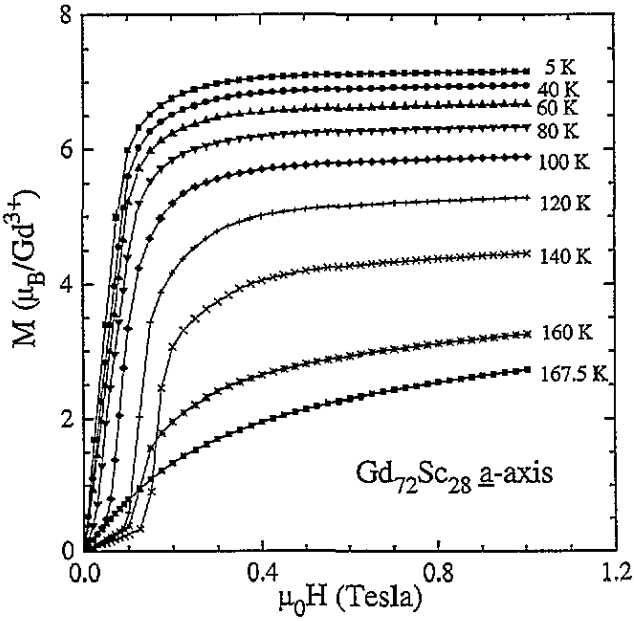

Figure 4. Magnetization as a function of applied magnetic induction for the a-axis $Gd_{72}Sc_{28}$ sample, at different temperatures.

magnetic spin system are much stronger for measurements parallel to the hexagonal c-axis since this is the direction of the magnetic periodic modulation.

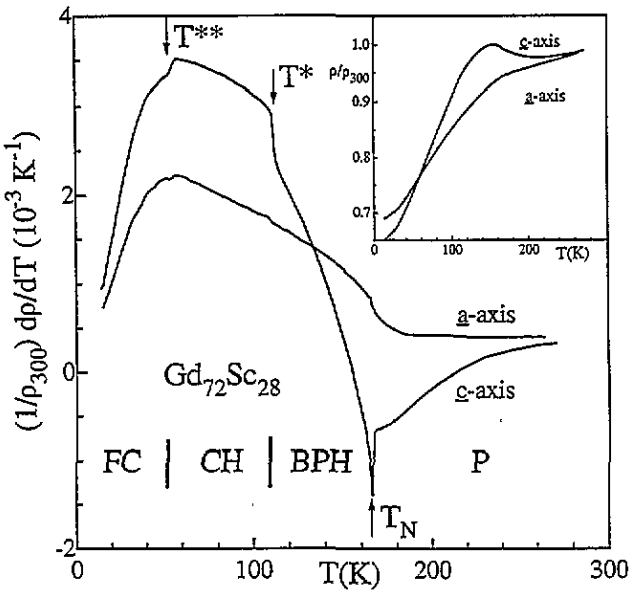

Figure 5. The normalized temperature derivative $((1/\rho_{300})(d\rho(T)/dT))$ of the electrical resistivity as a function of temperature for a- and c-axis $Gd_{72}Sc_{28}$ alloys. The transition temperatures are marked by vertical arrows. Inset: normalized electrical resistivity $(\rho(T)/\rho_{300})$ as a function of temperature for the same samples.

A small step anomaly is observed in $(d\rho/dT)_c$ at T_N, at the onset of the basal plane helix structure, preserving, however, the $\rho_c(T)$ continuity, thus indicating a second-order transition. At lower temperatures, the sudden increase in $(d\rho/dT)_c$ which occurs just below $T^* \cong 110$ K can be attributed to the onset of the c-axis ferromagnetic order (i.e. the transition from a basal plane helix to a conical helix), which decreases ρ, leading to a higher $d\rho/dT$ value. The subsequent development of the canted ferromagnet, starting at $T^{**} \cong 55$ K, is associated with a small step in $(d\rho/dT)_c$, but in the opposite sense to that observed at the basal–conical helix transition. This step can be understood if we recall that the helix turn angle, ω, gives a specific contribution to $d\rho/dT$ through $d\omega/dT$. As $d\omega/dT > 0$ above T^{**} and $d\omega/dT = 0$ below, we can understand the negative step in $(d\rho/dT)_c$ as T decreases through the transition.

In the paramagnetic phase, close to T_N, an upward curvature develops in $(d\rho/dT)_c$ similar to earlier observations in Gd–Y alloys [11] where the effect is attributed to the critical enhancement of short range c-axis order. As T approaches T_N a sudden crossover is observed in $(d\rho/dT)_c$ attributed to the rapid decrease of the c-axis fluctuations, enhancing the basal plane spin correlations and leading to the onset of the basal plane helical structure at T_N. This crossover occurs so close to T_N that the transition in $(d\rho/dT)_c$ looks almost a steplike anomaly.

3.3. Magnetoresistance $(\Delta\rho/\rho)$

We have studied the behaviour of the magnetoresistance in this alloy by measuring the changes in ρ_a as a function of a magnetic field parallel to the a-axis $[\Delta\rho(T, H) = \rho(T, H) - \rho(T, 0)]$. We first consider representative curves in each magnetic phase before presenting an overview for detailed comparisons.

Figure 6(a) shows a plot of $\Delta\rho/\rho$ and $d(\Delta\rho/\rho)/dH$ versus H, with measurements taken at 28.7 K, i.e. in the canted ferromagnetic phase. The magnetoresistance curve shows immediately ($H \geqslant 0$) a gradual decrease of $\Delta\rho/\rho$ with H, with a negative curvature (parabolic-like regime), leading to a strong minimum in the derivative $d(\Delta\rho/\rho)/dH$ at $\mu_0 H_{c1} \cong 0.04$ T. For $H > H_{c1}$, the curvature becomes positive and $\Delta\rho/\rho$ decreases more slowly towards saturation. These features are consistent with the behaviour of $M(H)$ showing a linear initial regime ($H < H_{c1}$) attributed to magnetic domain wall motion, followed by a rotation regime of the magnetic moments into the a direction, ultimately leading to saturation at high fields. Since one generally expects $\rho(T, H) \sim \rho_\infty\{1-[M(T, H)/M_0]^2\}$, the behaviour of $\Delta\rho/\rho$ and $d\rho/dH$ directly reflects the behaviour of M^2 and $M(dM/dH)$ respectively; for example, the initial parabolic behaviour of $\Delta\rho/\rho$ results from the initial linear field dependence of M at low fields.

The behaviour of $\Delta\rho/\rho$ and $d(\Delta\rho/\rho)/dH$ in the helix region is more complex, as illustrated in figure 6(b) for $T = 96.9$ K. We first notice that that $\Delta\rho/\rho$ is *almost* zero in low fields, indicating the initial stability of the helix structure. However, this stability *suddenly breaks down at* $\mu_0 H_{c1} = 0.057$ T, *with the collapse of the helix structure into* the fan phase [12]. This produces a step-decrease of $\Delta\rho/\rho$ at H_{c1} and an associated negative singularity in $d(\Delta\rho/\rho)/dH$, indicating a first-order induced magnetic transition. The critical field for this phase change (i.e. from the helix to the fan phase with a basal plane component; significant c-axis moment component rotation is not expected in low applied fields) correlates well with the value deduced from the sudden change in the slope observed in the magnetization curve (figure 4). After this transition $\Delta\rho/\rho$ exhibits an almost linear field dependence that is associated with the progressive closing of the fan and extends up to $\mu_0 H_{c2} \cong 0.15$ T [12, 13].

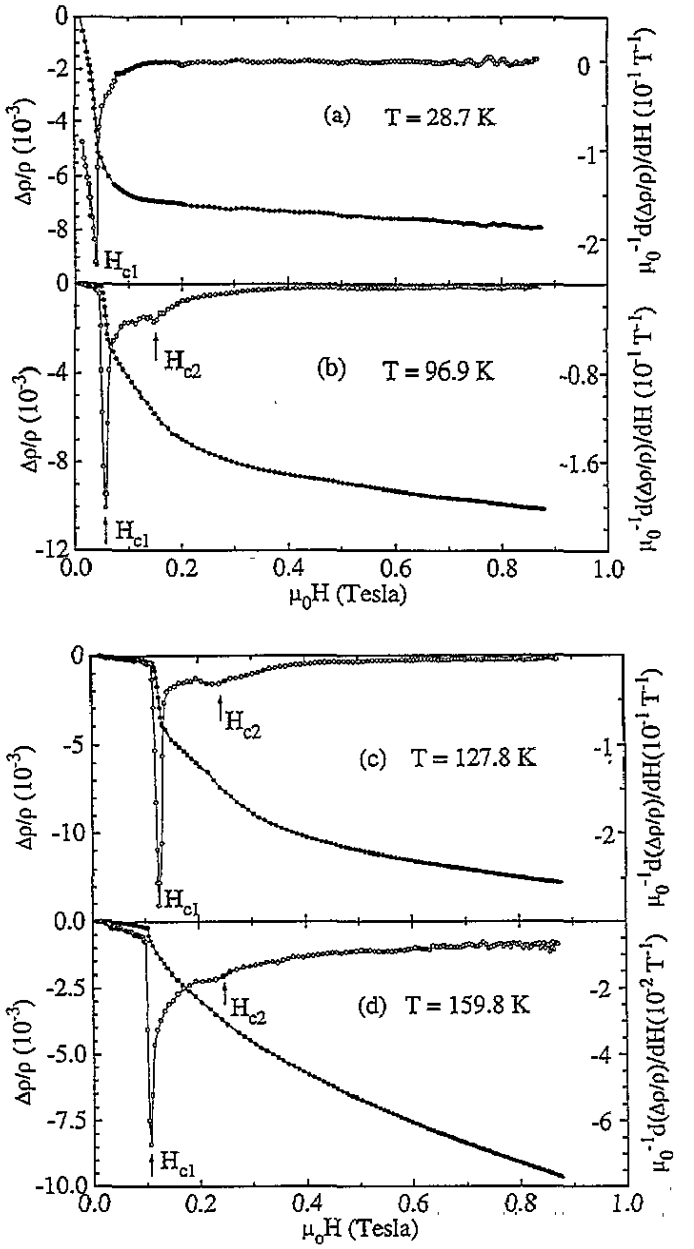

Figure 6. The magnetoresistance ($\Delta\rho/\rho$) (●) and its field derivative ($d(\Delta\rho/\rho)/dH$) (○) as a function of magnetic induction, for (a) $T = 28.7$ K (canted ferromagnetic phase), measured in the a-axis sample, (b) $T = 96.9$ K (conical helix phase), (c) $T = 127.8$ K (basal plane helix phase), (d) $T = 159.8$ K (basal plane helix phase, near the Néel temperature T_N).

At higher fields ($H > H_{c2}$) one expects a ferromagnetic phase with a random distribution of basal plane moments around the H direction, with the mean angular aperture directly controlled by the competition between the magnetic and thermal energy per ion. The remaining curvature observed in $\Delta\rho/\rho$ above 0.15 T reflects the final alignment of the basal

plane moment component and any remaining rotation of the *c*-axis component towards the basal plane.

In the basal plane helical region (figure 6(c)) at 127.8 K there is an initial field range where the helix is only slightly distorted by the field, as also happened in the conical helix. At $\mu_0 H_{c1} \cong 0.13$ T the helix collapses into the fan phase as evidenced by the sharp break in $\Delta\rho/\rho$ and the very narrow minimum in $d(\Delta\rho/\rho)/dH$ which occurs at H_{c1}. This is followed by a linear region in $\Delta\rho/\rho$ (extending up to ~0.24 T) over which the fan is slowly closing towards the *a*-axis. The end of this linear region marks H_{c2}. Above this field the curvature is less pronounced than in the conical helix, since there is no contribution from the *c*-axis moments.

Very close to T_N (figure 6(d)) at 159.8 K, the collapse of the helix into a fan phase is less dramatic (the spontaneous magnetization is much smaller here), suggesting a second-order phase transition. This is followed by an extended range of magnetic fields from 0.11 T up to $\mu_0 H_{c2} \cong 0.24$ T where the magnetic moments exhibit a smooth reorientation in the fan phase.

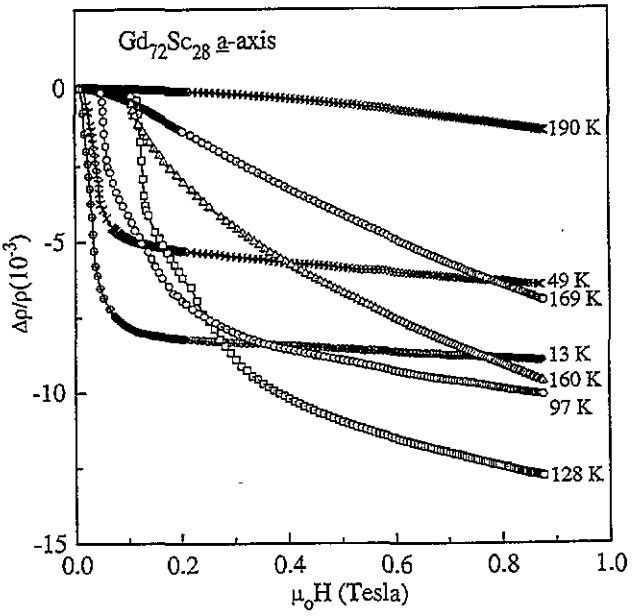

Figure 7. Isothermal $\Delta\rho/\rho$ curves as a function of applied magnetic induction, at different temperatures.

Figure 7 shows a composite illustration of selected isothermal field plots of $\Delta\rho/\rho$ illustrating the following.

(i) In the low temperature canted-ferro phases (the 13 K and 49 K curves), the initial drop in $\Delta\rho/\rho$ is continuous from $H \cong 0$, saturating rapidly with the transition to basal-plane ferromagnetism. The small slope of $\Delta\rho/\rho$ at high fields in the 13 K curve indicates fairly small spin disorder effects at these temperatures, giving an almost negligible paraprocess. For the curve taken at 49 K the high-field slope is greater, as expected for higher thermal disorder.

(ii) The conical helix (the curve at 97 K) structure 'resists' at low fields ($\Delta\rho/\rho \sim 0$), up to the first critical field $\mu_0 H_{c1} \cong 0.057$ T where a first-order transition occurs to a fan

phase. From our results it is not clear whether this transition brings the c-axis moments of the conical helix towards the basal plane (at H_{c1}) or whether a gradual rotation of such moments still occurs in the fan structure. In the fan phase we again observe an almost linear field dependence of $\Delta\rho/\rho$, before reaching the ferromagnetic phase at $\mu_0 H_{c2} \cong 0.15$ T. The magnetoresistance slope at high fields is now much higher than in the previous curves, due to the thermal enhancement of the spin fluctuations.

(iii) In the helimagnetic phase (curves at 128 K and 160 K) we see a very sharp break in the $\Delta\rho/\rho$ in the curve at 128 K $\mu_0 H_{c1} \cong 0.13$ T, indicating a strong first-order transition from the basal plane helix to the fan structure. These results agree with the theoretical prediction for temperatures considerably below T_N [14, 15]. In the curve at 160 K, corresponding to $T \cong 0.94\,T_N$, we observe a continuous transition at $\mu_0 H_{c1}$, although with a pronounced slope. This is again consistent with the theoretical prediction of a second-order phase transition when T is close to the Néel point [12, 13].

(iv) In the paramagnetic phase (190 K curve) we observe the usual quadratic field dependence, $\Delta\rho \sim H^2$, over the whole range of applied magnetic fields.

3.4. The magnetic H–T phase diagram

To summarize the information obtained from the magnetization and transport data, in figure 8 we give the magnetic phase diagram for $Gd_{72}Sc_{28}$ as a function of temperature and applied magnetic field. The conical field $H_{c1}(T)$, separating the initial distorted helix (or conical helix) from the corresponding fan structures [14, 15] was independently determined from first- and second-order field derivatives of the isothermal magnetization and magnetoresistance data. As shown in figure 8, the results are remarkably consistent. The $H_{c1}(T)$ phase line for $Gd_{72}Sc_{28}$ has the classical shape of the traditional rare earth elements such as Dy, Tb, etc [16]. We notice, however, an inflection point in the $H_{c1}(T)$ line which occurs at a temperature separating the conical helix from the basal plane helix regimes.

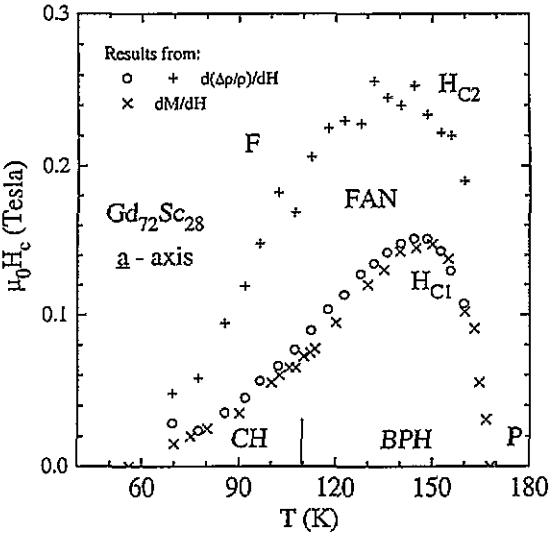

Figure 8. Magnetic H–T phase diagram for a-axis $Gd_{72}Sc_{28}$ sample.

The transition between the fan structure and the ferromagnetic phase is continuous and produces only a weak change in the magnetization slope, usually within the scatter of the experimental points. However, the very sensitive $\Delta\rho/\rho$ data enable us to identify the corresponding critical field (H_{c2}), through a steplike anomaly in the field derivative $d(\Delta\rho/\rho)/dH$ (see figures 6(c) and 6(d)). Theory predicts that H_{c2} should be approximately twice H_{c1} [16], a result which is consistent with our data.

Acknowledgments

J A Mendes is 'bolseiro de doutoramento' from JNICT. The authors thank Dr D Fort of Birmingham University for producing the single crystals used in this work. This work has been partially supported by Programa Ciência, contract 0058/C/91 and project STRDA/C/CEN/522/92.

References

[1] Melville R J, Palmer S B, Sousa J B, Moreira J M, Carvalho C and Pinto R P 1988 *J. Physique Coll.* **49** C8 341
[2] Melville R J, Palmer S B, McIntyre G J and Sousa J B 1988 *J. Appl. Phys.* **64** 5889
[3] Melville R J, Bates S, McIntyre G J, Sousa J B and Palmer S B 1988 *Europhys. Lett.* **6** 725
[4] Cable J W and Wollan E O 1968 *Phys. Rev.* **165** 733
[5] Melville R J, Bates S, McIntyre G J, Sousa J B and Palmer S B 1989 *Physica* B **156–157** 768
[6] Hellier A G, Palmer S B and Whitehead D G 1975 *J. Phys. E: Sci. Instrum.* **8** 352
[7] Salgueiro da Silva M, Eccleston R S, Sousa J B and Palmer S B 1992 *Ultrasonics* **30** 347
[8] Moreira J M 1985 *PhD Thesis* Porto
[9] Sousa J B and Moreira J M 1985 *Portugaliae Physica* **16** 191
[10] Elliott R J 1972 *Magnetic Properties of Rare Earth Metals* (London: Plenum)
[11] Sousa J B, Moreira J M, Braga M E, Palmer S B, Bates S and Beaudry B J 1984 *J. Phys. F: Met. Phys.* **15** 1171
[12] Nagamiya T, Nagata K and Kitano Y 1962 *Prog. Theor. Phys.* **27** 1253
[13] Kitano Y and Nagamiya T 1964 *Prog. Theor. Phys.* **31** 1
[14] Yamada H and Takada S 1972 *Prog. Theor. Phys.* **48** 1828
[15] Yamada H and Takada S 1973 *Prog. Theor. Phys.* **49** 1401
[16] Coqblin B 1977 *The Electronic Structure of Rare Earth Metals and Alloys: The Magnetic Heavy Rare Earths* (London: Academic)